경계 요소법을 이용한 2차원 비등방성 복합재료 탄성체의 비파괴 결함 추정

Nondestructive Defect Detection in Two-dimensional Anisotropic Composite Elastic Bodies Using the Boundary Element Method

이 상 열†
Lee, Sang-Youl
(논문접수일 : 2003년 7월 25일 ; 심사종료일 : 2004년 3월 5일)

요 지

본 연구에서는 경계 요소법을 이용하여 2차원 비등방성 탄성체의 손상 규명을 수행한다. 경계에서의 적분항만을 포함하는 본 수치모델은 1차원으로 줄게된다. 이러한 장점은 특히 균열 역학과 같은 문제에 있어서 중요한 의미를 갖는다. 또한 일정 영역을 분할하는 기법을 피함으로서 수치해석 과정을 간편하고 효율적으로 수행할수 있기 때문에 역문제 해결에 있어서 장점을 갖는다. 본 연구에서는 기존의 등방성 재료에 대한 비파괴 추정기법을 복합신소재와 같은 비등방성 재료로 이루어진 탄성체의 해석에 대하여 확장한다. 먼저 경계요소법에 의한 수치모델의 타당성을 기존의 문헌과 비교 검증하며, 서로 다른 특성을 보이는 비등방성 형식의 변화에 따라 실제 측정시 발생하는 노이즈 영향을 분석한다. 수치예제는 적층 형태 및 하중조건에 대하여 수행하며, 결함 추정에 미치는 적층 형태의 영향을 시험한다.

핵심용어 : 경계요소법, 역 문제, 비등방성 재료, 노이즈 영향, 결함 추정

Abstract

In this paper, the defects of two-dimensional anisotropic elastic bodies are identified by using the boundary element method. The use of numerical models that contain only boundary integral terms reduces the dimensionality of the problem by one. This advantage is particularly important in problems such as crack mechanics. Avoiding domain meshing is also particularly advantageous in the solution of inverse problems since it overcomes mesh perturbations and simplifies the procedure. In this paper, nondestructive approaches for the existing isotropic materials are extended to analyze the elastic bodies made of anisotropic materials such as composites. After verifying that the proposing boundary element model is in good agreement with numerical results reported by other investigators, the effect of noise in the measurements on the identifiability is studied with respect to different design parameters of layered composites. Sample studies are carried out for various layup configurations and loading conditions. The effects of the layup sequences in detecting flaw of composites is explored in this paper.

Keywords : *boundary element method, inverse problem, anisotropic material, noise effect, defect detection*

1. Introduction

With the advancement of technology in fiber-reinforced composite materials, the applicability of composites to structural members has been increased significantly due to their merits such as low density, high stiffness and high strength. Consequently, the need for safe monitoring and predictive nondestructive evaluation (NDE) and other inverse problems in such sensitive and expensive structures

† 책임저자, 정회원 · MIT 토목환경공학과 박사후연구원
전화: 1-617-258-8366; Fax: 1-617-253-6044
E-mail: leesy@mit.edu

• 이 논문에 대한 토론을 2004년 6월 30일까지 본 학회에 보내주시면 2004년 9월호에 그 결과를 게재하겠습니다.

is constantly increasing.

In some class of inverse problems, the use of the BEM provides clear advantages in comparison with the finite element method and others. First, it does not require a remesh of the domain of the body at each iteration. This reduces both the computational effort and eliminates small but important perturbations due to the changes of the mesh. Second, the application of these methods to real problems may require many iterations, as well as high precision in the intermediate solutions, so the use of finite elements would be very expensive.

Structural analysis of anisotropic composite materials using the boundary element method (BEM) has been studied previously by a number of investigators. The first application of the BEM for composite materials was made by Cruse and Swedlow[1] in 1971. Later, the formulation was extended to two -dimensional crack problems by Cruse and Snyder[2] and a general three-dimensional problem was presented by Cruse and Willson.[3] The first extension to two-dimensional elastodynamic in the time domain was developed by Wang *et al.*[4] in 1996. Other application of BEM for adhesively bonded patches can be found in Young *et al.*[5] Recently, Lingyun *et al.*[6] analyzed two-dimensional micro mechanical behaviors of composite materials using BEM. A new boundary element formulation for the mechanically fastened composite patch was developed by Widagdo and Aliabadi.[7]

For inverse defect identification, in comparison to standard imaging techniques, we reduce the output data from the classical complete bitmap of the image to a reduced set of parameters that gives an univocal description and characterization of the defect. The basic concept of parametrization is based on defining the flaw geometry by a reduced set of parameters P, which becomes the unknown of the inverse problem. In identification problems, the geometry is usually defined by simple geometrical entities, in turn defined by a few parameters.[8),9)]

To solve the inverse problem, we choose the procedure[10] based on the minimization of the discrepancy between measured and predicted response. In this paper, the previous concepts are extended from isotropic materials to anisotropic multilayered composite materials.

2. Theoretical formulation

Fig.1 shows the structural and material axes of a two-dimensional anisotropic body.

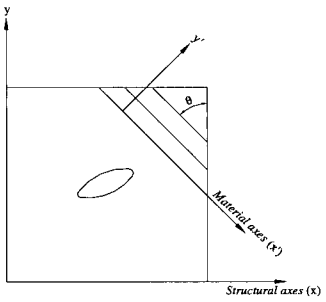

Fig.1 Structural and material axes

From Fig. 1, the transformed tensor σ_{ij} of the plane stresses σ_{pq} between the structural and material axes is

$$\sigma_{ij} = l_{ip}\sigma_{pq}l_{qj} \qquad (i,j,p,q=1,2,6), \tag{1}$$

where, l_{ij} is a transformation matrix. The relationship between the displacement vector u_i and the linear strain tensor ε_{ij} is given through the compatibility equation,

$$\varepsilon_{ij} = \frac{1}{2}(u_{i,j} + u_{j,i}) \tag{2}$$

In the generalized Hooke's law, a two-dimensional anisotropic composite material stiffness C_{ij} and flexibility a_{ij} can be expressed in the following convenient form using the single-subscript notation for stress and strain components and the double -subscript notation for elastic constants:

$$\sigma_i = C_{ij}\varepsilon_j \qquad \varepsilon_i = a_{ij}\sigma_j \qquad (i,j=1,2,6) \tag{3}$$

Following the notation of Lekhnitskii[11], the flexibility matrix a_{ij} in terms of engineering constants can be written as

$$[a_{ij}] = \begin{bmatrix} 1/E_1 & -\nu_{21}/E_2 & 0 \\ -\nu_{12}/E_1 & 1/E_2 & 0 \\ 0 & 0 & 1/G_{12} \end{bmatrix} \tag{4}$$

where E_1, E_2, ν_{12}, ν_{21}, and G_{12} denote elastic modulus, Poisson's ratio, and shear modulus, respectively. Combining Eqs.(1), (2), and (3) by using transformation from the material coordinate system, the stress-strain relationship in global coordinate system follows as

$$\bar{\sigma}_i = l_{ij}\sigma_j = l_{ij}C_{ij}\varepsilon_j = l_{ij}C_{ij}l_{ij}^T\,\bar{\varepsilon}_{ij} = \bar{C}_{ij}\,\bar{\varepsilon}_j, \tag{5}$$

$$\bar{\varepsilon}_i = \bar{a}_{ij}\,\bar{\sigma}_j \tag{6}$$

In order to analyze a multilayered anisotropic material we model the combination of single layers as follows. We proceed deriving the constitutive equations that relate the force resultants to the strains of a laminate. Eq. (6) holds for the kth lamina in the problem coordinates. The integration of stresses through the laminate z-thickness requires lamina wise integration. Hence, the force resultants N_i (i= 1, · · ·,n) are given by[12]

$$N_i = \sum_{k=1}^{n}\int_{z_k}^{z_{k+1}}\sigma_i dz = \sum_{k=1}^{n}\int_{z_k}^{z_{k+1}}\bar{C}_{ij}\varepsilon_i = A_{ij}\varepsilon_j \tag{7}$$

$$\varepsilon_i = \bar{A}_{ij}\,N_j \tag{8}$$

where n is the number of layers. For the two-dimensional analysis of a generally anisotropic medium, the fundamental solutions are given by the following closed forms.

In Eq. (9), u_j^i and q_i^j are the j^{th} components of the displacement and traction at the observation point due to a singular load at a distance z toward direction i.

$$u_i^j = 2Re[A_{i1}B_{j1}\ln z_1 + A_{i2}B_{j2}\ln z_2] \tag{9}$$

$$q_i^j = 2Re[\frac{A_{i1}C_{j1}}{z_1}(\mu_1 n_1 - n_2) + \frac{A_{i2}C_{i2}}{z_2}(\mu_2 n_1 - n_2)]$$
$$(i,j=1,2) \tag{10}$$

where μ_k are the complex roots of the characteristic polynomial,

$$a_{11}\mu^4 - 2a_{16}\mu^3 + (a_{12}+a_{66})\mu^2 - 2a_{16}\mu + a_{22} = 0 \tag{11}$$

and complex constants B_{kl} in Eq. (10) are given as follows,

$$\begin{aligned} B_{1l} &= a_{11}\mu_l^2 + a_{12} - a_{16}\mu_l \\ B_{2l} &= a_{12}\mu_l^2 + a_{22}\mu_l - a_{26} \end{aligned} \tag{12}$$

$C_{1k}=\mu_k$, $C_{2k}=-1$, and A_{kl} are also the complex roots that is obtained from the following equation.

$$\begin{bmatrix} 1 & -1 & 1 & -1 \\ \mu_1 & -\bar{\mu}_1 & \mu_2 & -\bar{\mu}_2 \\ B_{11} & -\bar{B}_{11} & B_{12} & -\bar{B}_{12} \\ B_{21} & -\bar{B}_{21} & B_{22} & -\bar{B}_{22} \end{bmatrix} \begin{Bmatrix} A_{k1} \\ \bar{A}_{k1} \\ A_{k2} \\ \bar{A}_{k2} \end{Bmatrix} = \begin{Bmatrix} \delta_{k2}/2\pi i \\ \delta_{k1}/2\pi i \\ 0 \\ 0 \end{Bmatrix} \tag{13}$$

3. Boundary element method

The integral equation we use for the BEM is one that directly relates u_i and p_i. For the equilibrium equation ($\sigma_{ij,j}+b_i=0$) at any point of a domain Ω enclosed by a boundary Γ, the principle of the inner product or weak formulation is given as

$$\int_\Omega(\sigma_{ij,j}+b_i)w_i d\Omega = 0 \tag{14}$$

where w_i is the ith weight function. If we choose the previously obtained fundamental solution u_k^i as the kernel function and integrate it by parts twice the first component, we obtain Betti's reciprocity theorem:

$$\int_\Omega(\sigma_{ik,j}^i u_k)d\Omega + \int_\Omega b_i u_k^i d\Omega = -\int_\Gamma \sigma_{jk}n_j u_k^i d\Gamma + \int_\Gamma \sigma_{jk}^i n_j u_k d\Gamma \tag{15}$$

The reason for choosing a singular fundamental solution is that the identity $\sigma_{jk,j}^i + \delta(y-x)e_i = 0$ (where y is the pole and x is the observation point), converts the first domain integral into a single-point value (the kernel is zero-valued everywhere excepting at the pole), giving:

$$-u_i(y) + \int_\Omega b_i u_k^i d\Omega = -\int_\Gamma \sigma_{jk}n_j u_k^i d\Gamma + \int_\Gamma \sigma_{jk}^i n_j u_k d\Gamma \tag{16}$$

Neglecting body forces in Eq. (16), the integral equation at the boundary is obtained:

$$u_i(y)+\int_\Gamma (q_k u_k^i - q_k^i u_k)d\Gamma \tag{17}$$

Eq. (17) can be turned into a boundary integral equation if we take the pole x_i to the boundary. In this case the integrals can turn singular. After a careful limiting process, the Eq. (17) turns into:

$$c_k^i u_k(y)+\int_\Gamma [q_k^i(y,x)u_k(x)-u_k^i(y,x)q_k(x)]d\Gamma(x)=0 \tag{18}$$

where the integrals have the sense of *Cauchy Principal Value*, which has to be evaluated numerically by using so-called regularization techniques.[13] Any of the equations above are valid for a continuum problem. As mentioned earlier we express the continuum in terms of discrete values by

$$x_k=\sum\phi_j x_j^k,\quad u_k=\sum\phi_j u_j^k \quad \text{and} \quad q_k=\sum\phi_j q_j^k \tag{19}$$

A determined system of equation is constructed writing the boundary integral equation once for every collocation point and direction. The system is then reorganized so as to include all unknown displacements u_i and tractions q_i in vector v.

$$\mathrm{Hu}=\mathrm{Gq};\quad \mathrm{Av}=\mathrm{b} \tag{20}$$

4. Inverse problem and identification

The concept of identifiability has to be defined within the context of the complete solution of an inverse problem.

The preceding BEM model is used in an inverse solution strategy based on minimization of discrepancy. First, the specimen is loaded with a specific case in order to provoke a clearly measurable deformation. The static deformed shape is measured at all points and directions at the boundary. The detection is then based on the minimization of a residual between the amplitudes $v^{\exp}$ at the receiver transducers and the computed predictions v of them by this method. The latter are functions of the parameters P_g that describe the flaws as shown in Table 1.

The central idea of the inverse solution is the optimization of a cost functional with respect to the parameters P_g. The cost functional is defined in a least squares sense. The residual vector R and function L are written as

$$R=v^{\exp}-v \qquad L=\frac{1}{2}R^T R \tag{21}$$

In the following, instead of minimizing L, we define the cost function f as a value to be maximized:

$$f=-\log(L+r) \tag{22}$$

where r is error in measurements. The reason for this choice is that it is better suited and gives better results when applied to certain optimization techniques such as genetic algorithms.[14),15)]

For the parameterization scheme we make use of a field of deformation $\bar{x}_i$ defined in the introduction as a vectorial field, expressing the change of position of each material point.

For our particular case, we have chosen a very simple nonlinear parameterization capable of representing defects assuming any elliptical shape, size and orientation:

$$\bar{x}_i(P_g)=\begin{bmatrix} P_1+(P_3\cos P_5-P_4\sin P_5) \\ P_2+(P_3\cos P_5+P_4\sin P_5)\end{bmatrix} \tag{23}$$

Table 1 Definition of the parameter vector Pg.

Parameter	Definition
x_1^{cg}(P1)	Horizontal coordinate of the centroid of the defect
x_2^{cg}(P2)	Vertical coordinate of the centroid of the defect
a(P3)	Horizontal size
b(P4)	Vertical size
α(P5)	Angle of rotation (radians)

5. Numerical results and discussion

5.1 Numerical model and verification of results

In this paper, two models which are combinations of two specimen shapes under two different load cases each are used, as shown in Fig. 2. They consist of rectangular plates of layered composite materials under aligned loads, which makes them 2D problems. Since the defects have close to null stiffness properties, they are correctly modeled as elliptical holes of a variable angle, size and position, which are to be determined.

The material is a layered composite with a variable number of layers and a specific sequence of cross or angle ply. The properties of composite materials in this study are listed in Table 2. Due to the large amount of parameters to study, the procedure will be to keep one parameter fixed while moving the rest. 40 quadratic elements evaluated using 8-point gauss quadrature each are used. The unknowns and collocation points are placed according to the scheme of conforming elements.[13] In addition, a dimensionalization scheme for all the magnitudes toward unity values has been used. It works introducing a new system of magnitudes and establishing the necessary correspondence with the input system. The motivation is to overcome numerical instabilities of the inversion procedure introduced in Ref. [2] and [14].

Table 2 Material properties used in this study.

Materials	E1(GPa)	E2(GPa)	G12(GPa)	v12
Graphite-Epoxy (AS/3501)	137.90	8.96	7.10	0.30
Glass-Epoxy	53.78	17.92	8.96	0.25

The boundary element formulation described earlier is now implemented to compare the results in the isotropic case with unity Young's modulus and 0.3 Poisson ratio computed by Rus and Gallego.[15] The present anisotropic code is used in a limited procedure since completely isotropic elastic properties are not valid in this formulation. The problem is depicted as well as the points from which the comparison data have been taken are represented in Fig. 3 and Table 3. The values in Table 3 are appropriately coincident (errors within 3.5% for the chosen 40-elements discretization), giving enough confidence on the boundary element code.

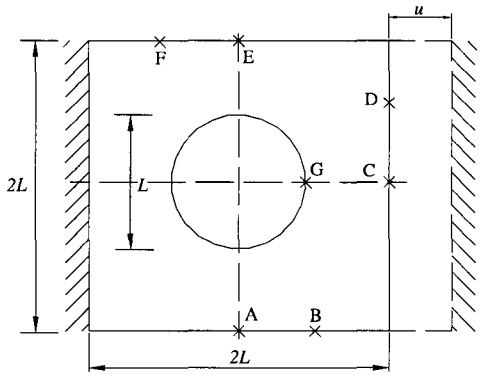

Fig. 3 Definition of points for comparison (Load case II).

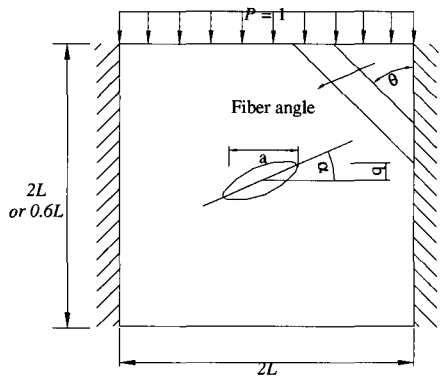

(a) Load case I

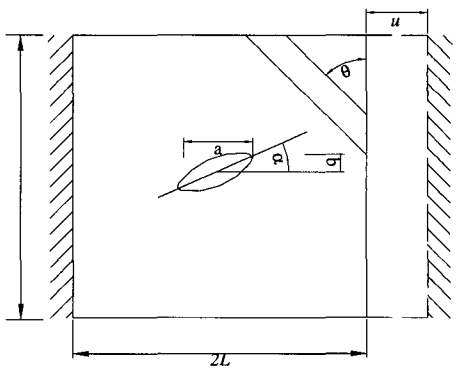

(b) Load case II

Fig. 2 Description of numerical models.

Table 3 Comparison of displacements/tractions computed by Rus&Gallego and present study.

	Ref.[15]		This study		Error(%)	
Point	x	y	x	y	x	y
A	0.500	0.309	0.500	0.274	0.00	3.51
B	0.696	0.178	0.695	0.146	0.04	3.21
C	0.054	0.000	0.049	0.000	0.56	0.00
D	0.307	-0.041	0.277	-0.036	2.99	0.50
E	0.500	-0.309	0.500	-0.275	0.00	3.39
F	0.304	-0.178	0.305	-0.147	0.08	3.17
G	0.998	0.000	0.099	0.0001	0.35	0.01

5.2 Noise effects

The identifiability through analyzing the cost functional f in Eq.(22) versus the value of the parameter with noises is first examined. The noise in the measurements is varied by using a Gaussian distribution with zero mean. The cost functional f should be a maximum value when it is close to the real position, which we set to: $x_1^{cg}=0.10$, $x_2^{cg}=0.20$, a=0.30, b=0.20 and a=0.40.

Fig. 5 shows the values of the cost function versus the rotation angle of the flaw for two composite materials, for increasing unexpected noise. From Fig. 5 it may be noted that the glass-epoxy case gives somewhat better sensitivity, which we see from the fact that the cost function has a larger range of values. For 2% to 5% noise it is still possible to find a close value for the glass-epoxy model whereas it is not possible in graphite-epoxy. A search algorithm is more likely to find that maximum simply because the maximum is noticeably higher than the neighbour values, and in this case the maximum is much closer to the real value, and more distinguishable. A very interesting observation in graphite-epoxy is that the fitness function shows

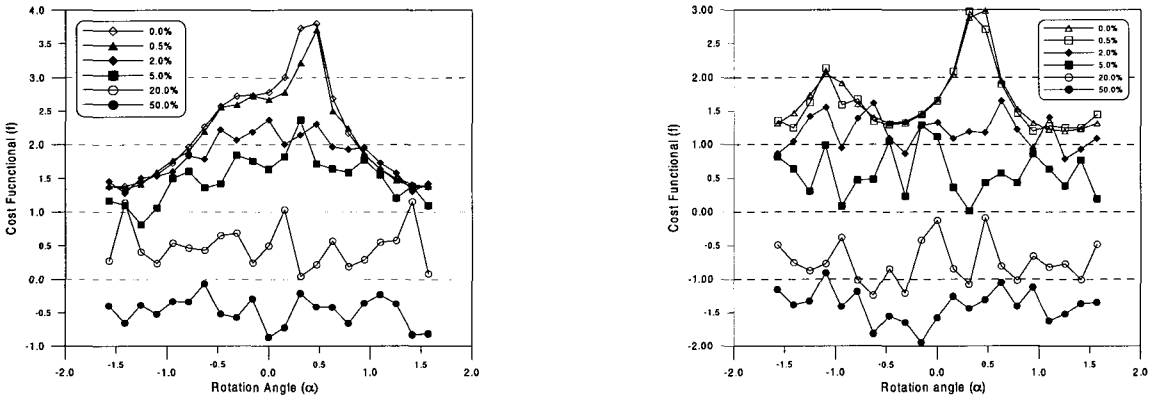

(a) Grass-Epoxy (b) Graphite-Epoxy

Fig. 4 Noise effects for Rotation angles in measurements (Load case I, [45/0/0/45]).

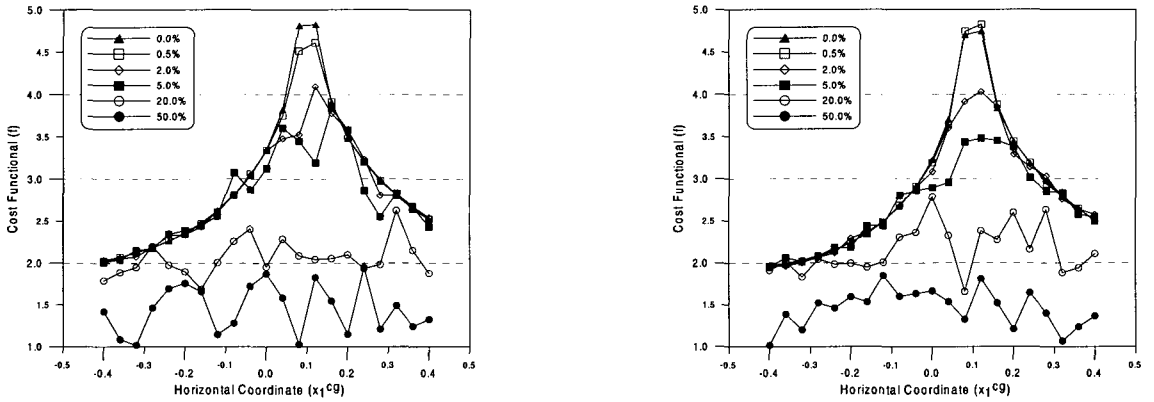

(a) [45/0/0/45] (b) [45/0/45]

Fig. 5 Noise effects for horizontal position in measurements (Load case I, Graphite-epoxy).

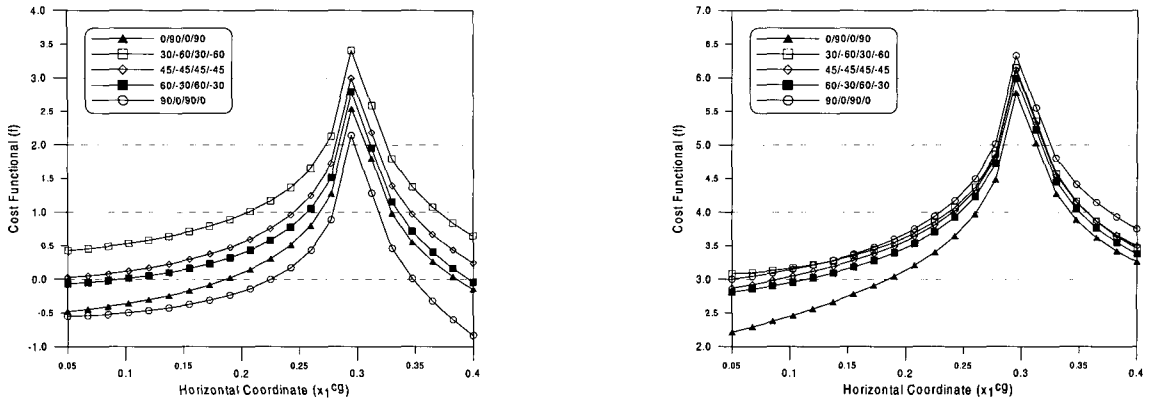

(a) Load case I (b) Load case II

Fig. 6 Horizontal position of the hole in detection. (Graphite-epoxy, 0% Noise).

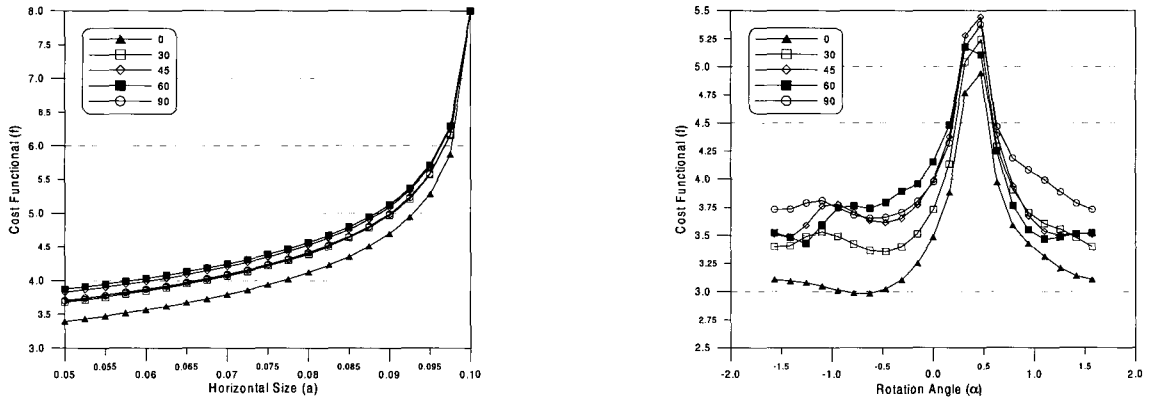

(a) [30/a/a/30], horizontal size (b) [60/a/a/60], rotation angle

Fig. 7 Detections for different layup sequences. (Graphite-epoxy, load case II, 0% Noise, a=0~90).

a secondary maximum which means that there is a different angle that gives almost the same response as the original one, which may lead to a false guess of the absolute maximum for 2% noise. It is remarkable that in the glass-epoxy, a shallower second maximum tends to appear at a different position, varying from angle -0.3 radians to -1.1 in graphite-epoxy. Fig. 6 shows the evolution of the identification cost function when the flaw is moved horizontally in composites with four different symmetric angle-ply layups. It may be observed that the 1 and 2 layer setups are less sensitive to the noise.

5.3 Effects of layup sequence

Fig. 7 shows the cost functional against the horizontal defect size in cross-ply composites with different fiber angles. In combination with the load case, the results obtained without noises could be noticeably different depending on the given fiber angles. The models with fiber angles 30° and 45° are easy to examine in load case 1, whereas the 90° model is very difficult. It is easy to understand that the lower levels of the cost function make it less capable to stand out among the noises. It may also be observed that load case 2 is less sensitive to the configuration of the fiber angles loadcase 1.

Fig. 8(a) shows the horizontal defect size in symmetric angle-ply composites by using different fiber angles. As shown in the figures, [30/60/60/30] gives the best identifiability, but not far ahead of the rest, excepting the [30/0/0/30]. The differences of the values in different fiber angles are almost at the same range of values. We may conclude from these results that the use of different layer sequences make little differences for the identification of the size. Fig. 8(b) also shows a similar case as above but for a different combination of fiber angles.

From the figure, it can be observed that [60/45/45/60] presents the best identifiability as opposed to [60/0/0/60]. It may be also noted that the position of a secondary maximum (≒-1.0~-1.5 radians) appears at different positions for different angles, which is closely related to the anisotropic nature of the composite materials.

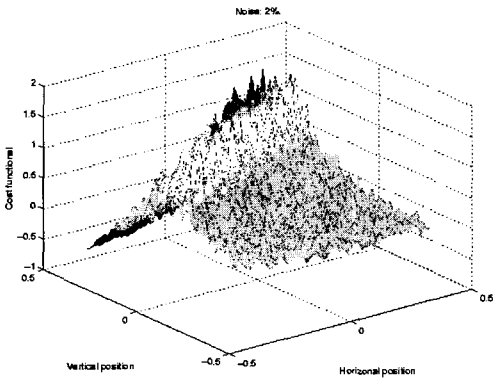

(a) 2% Noise

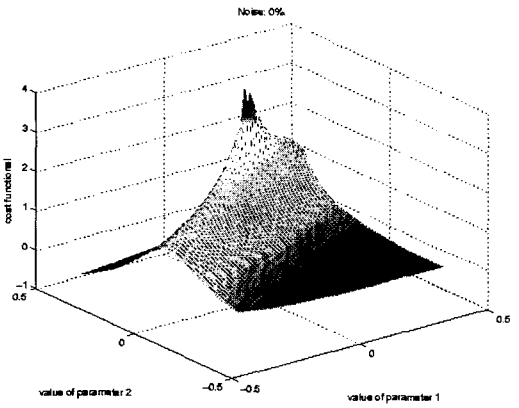

(b) Noise free

Fig. 9 Combination of horizontal and vertical coordinates of the damage (Graphite-epoxy, load case I).

5.5 Combination of parameters

Fig. 9 show the perspectives for the variation of the cost functional with two parameters at the same time. It is noted that there are some correlations between the parameters which makes it more difficult to find the exact position of the defect in that zone. It can be understood conversely that it is particularly easy to distinguish the location perpendicularly to that direction.

6. Summary and conclusion

An inverse technique is developed to identify various properties of anisotropic composites. For the numerical simulation of the problem, the boundary element technique has been used. It is an attractive approach, not only because it is computationally efficient and accurate but also because we can avoid the domain meshing that is mandatory in FEM. The technique is then implemented for anisotropic composites of various layup sequences to compare the results obtained from different noises and load cases. The results obtained from the boundary element formulation for isotropic structure are compared with the results available in the open literature and a good agreement is observed. In the numerical results, we observe that the use of different number of layers make little difference for detecting the sizes or positions regardless of fiber angles, but the difference becomes significant for the loading conditions and noise effects. This study may conclude that the effect of loading conditions and noises, largely governing the identification of composite structures, as well as the various fiber angles, should not be neglected. All these should be used to analyze and design the NDE setup, and even be taken into account for the composite design, pursuing a better accuracy of the detection.

References

1. Cruse T. A. and Swedlow J. L., Interactive program for analysis and design problems in advanced composites technolog, *AFML-TR-71-268, Carnegie-Mellon University*, 1971
2. Snyder M. D. and Cruse T. A., "Boundary-integral equation analysis of cracked anisotropic plates", *Int. J. Fract.*, Vol. 11, No. 2 1975, pp.315~328
3. Wilson R. B. and Cruse T. A., "Efficient implementation of anisotropic three dimensional boundary integral equation analysis", *Int. J. Numer. Meth. Eng.*, Vol. 12, No. 9, 1978, pp.1383~1397
4. Wang C. Y., Achenbach J. D. and Hirose S., "Two-dimensional time domain beam for scattering of elastic waves in solids of general anisotropy", *Int J Solids Struct.*, Vol. 22, No. 26, 1996, pp.3843~3864.
5. Young A., Rooke D. P. and Cartwright D. J., "Analysis

of patched and stiffened cracked panels using the boundary element method", *Int J Solids Struct.*, Vol. 29, No. 17, 1992, pp.2201~2216

6. Lingyun P., Daniel O. A. and Frank J. R., "Boundary element analysis for composite materials and a library of green's functions", *Comp Struct.*, Vol. 66, No. 5, 1998, pp.685~693
7. Widagdo D. and Aliabadi M. H., Boundary element analysis of cracked panels repaired by mechanically fastened composite patches, *Int. J. Eng. Anal. B. E.*, Vol. 25, No. 339, 2001, p.45
8. Bezerra L. M. and Saigal S., "A boundary element formulation for the inverse elastostatics problem of flaw detection", *Int. J. of Numer Meth Eng.*, Vol. 36, 1993, pp.2189~2202
9. Mellings S. C. and Aliabadi M. H., "Flaw identification using the boundary element method", *Int. J. of Numer Meth Eng.*, Vol. 38, 1995, pp.399~419
10. Gallego R. and Suarez J., "Numerical solution of the variation boundary integral equation for inverse problems", *Int. J. Numer Meth Eng.*, Vol. 49, 1999, pp. 501~518
11. Lekhnitskii S. G., *Theory of Elasticity of an Anisotropic Body*, MIR Publishers, Moscow, 1981
12. Lee S. Y., Baik H. S. and Chang S. Y., "A Numerical Comparison Study on Natural Vibration and Mode Characteristics of Anisotropic Laminated Composite Plates", *J. KSCE*, Vol. 20, 3-A, 2000, pp.357~366
13. Dominguez J., *Boundary Elements in Dynamics*, Elsevier, CMP, 1993
14. Rus G., *Numerical methods for nondestructive identification of defects*, PhD thesis, University of Granada, 2001
15. Rus G. and Gallego R., "Optimization algorithms for identification inverse problems with the boundary element method", *Int. J. Eng. Anal. B. E.*, Vol. 26, No. 4. 2002, pp.315~327